nature geoscience

LETTERS

PUBLISHED ONLINE: 26 JUNE 2011 | DOI: 10.1038/NGEO1188

Stronger ocean circulation and increased melting under Pine Island Glacier ice shelf

Stanley S. Jacobs[1]*, Adrian Jenkins[2]*, Claudia F. Giulivi[1] and Pierre Dutrieux[2]

In 1994, ocean measurements near Antarctica's Pine Island Glacier showed that the ice shelf buttressing the glacier was melting rapidly[1]. This melting was attributed to the presence of relatively warm, deep water on the Amundsen Sea continental shelf. Heat, salt and ice budgets along with ocean modelling provided steady-state calving and melting rates[2,3]. Subsequent satellite observations and modelling have indicated large system imbalances, including ice-shelf thinning and more intense melting, glacier acceleration and drainage basin drawdown[4–10]. Here we combine our earlier data with measurements taken in 2009 to show that the temperature and volume of deep water in Pine Island Bay have increased. Ocean transport and tracer calculations near the ice shelf reveal a rise in meltwater production by about 50% since 1994. The faster melting seems to result mainly from stronger sub-ice-shelf circulation, as thinning ice has increased the gap above an underlying submarine bank on which the glacier was formerly grounded[11]. We conclude that the basal melting has exceeded the increase in ice inflow, leading to the formation and enlargement of an inner cavity under the ice shelf within which sea water nearly 4 °C above freezing can now more readily access the grounding zone.

In the eastern Amundsen Sea (Fig. 1), Circumpolar Deep Water (CDW) intrudes onto the continental shelf at depths >300 m, salinities >34.6 and temperatures >3.5 °C above the freezing point ($T - T_f$, Fig. 2a). A thermocline (halocline) defined by strong vertical temperature (salinity) gradients lies between the relatively warm, salty CDW and colder, fresher surface waters. Although water in and above the resulting pycnocline (density gradient) is cooled and modified by sea surface processes, the CDW warmth and large areas of fast ice prevent formation of the cold, high-salinity shelf water that characterizes most other sectors of the Antarctic continental shelf. The new measurements show the pycnocline deepening southward into Pine Island Bay (PIB), then rising within a persistent cyclonic gyre also delineated by shipboard Acoustic Doppler Current Profiling (ADCP). Outer continental shelf sills may preferentially channel CDW across the shelf break[12,13], but a persistent temperature maximum extending southward from the upper CDW in Fig. 2a suggests inflows well above the sea floor. Temperature and salinity decrease by ~0.5 °C and 0.05 along the 27.75 isopycnal surface, with most of that change occurring over the outer shelf. Autosub mapped seawater properties beneath the Pine Island Glacier ice shelf (PIG), finding the same isopycnal directly above the crest of a 300 m-high, 700 m-deep submarine ridge transverse to the ice flow direction[11]. The properties of sea water with access to the PIG grounding zone differ little from those in the upper CDW >400 km away.

Combining the 2009 measurements with observations in 1994, 2000 and 2007 illustrates the subsurface summer thermohaline

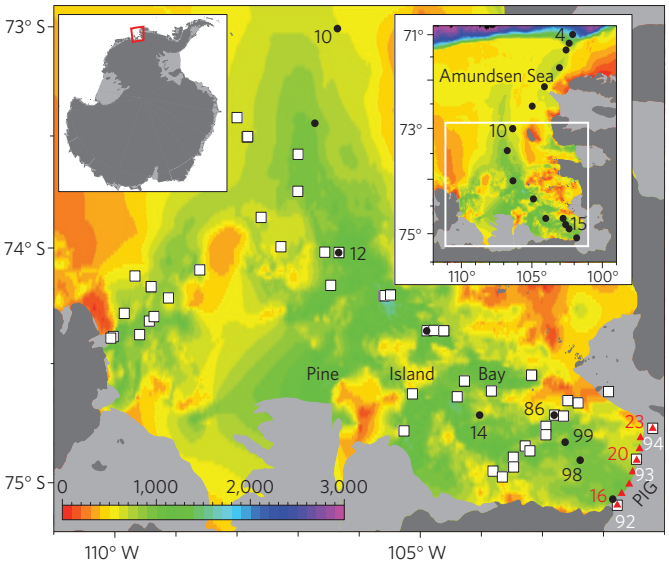

Figure 1 | Ocean stations in the eastern Amundsen Sea and greater PIB (>~74° S). Bathymetry and coastline[24] are zoomed out on the insets. Black dots are the 2009 CTD profiles in Fig. 2a; red triangles the 2009 CTDs 16-23 in Figs 2b, 3b and 4. White squares are paired CTDs from 1994, 2000, 2007 and 2009 (Fig. 3). Water column profiling included dissolved oxygen, and LADCP measurements after 1994.

structure in greater PIB and its interannual variability (Fig. 3a). Paired conductivity–temperature–depth (CTD) profiles at Fig. 1 sites, depth-averaged each year, show the coldest and freshest conditions in 2000 and the warmest and saltiest in 2009 along most pressure and isopycnal surfaces. At potential temperatures of −1 to +1 °C and pressures of 200–700 dbar, the thermocline was ~0.45 °C warmer on average in 2007/2009 and had shoaled everywhere since 1994/2000, at some levels by more than 100 dbar. Modelled isopycnal layer depths in PIB have suggested similar variability at interannual to decadal timescales[14]. Variability decreases sharply below the thermocline, with CDW temperatures ~0.1–0.2 °C higher in 2007/2009 than in 1994/2000. These observations indicate a greater volume of slightly warmer CDW in PIB during recent summers, and the largest thermohaline changes in the overlying pycnocline.

CDW clearly dominates the lower water column in the eastern Amundsen, is amply supplied from the continental shelf break region and extends largely unperturbed into the outer cavity beneath the PIG (Fig. 2a). Its small temperature increase in recent years may reflect warming in the vast upper CDW reservoir north of the shelf break. Although that change appears inadequate to account

[1]Lamont-Doherty Earth Observatory of Columbia University, Palisades, New York 10964, USA, [2]British Antarctic Survey, Natural Environment Research Council, Cambridge, CB3 0ET, UK. *e-mail: sjacobs@ldeo.columbia.edu; ajen@bas.ac.uk.

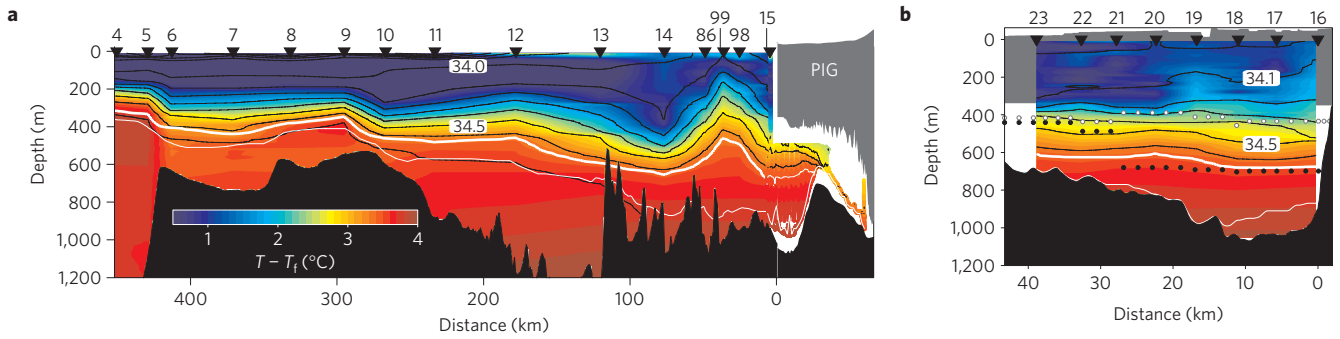

Figure 2 | Vertical temperature and salinity sections. a,b, Vertical temperature and salinity sections (**a**) from the CTDs shown in the Fig. 1 inset and extended beneath the PIG and (**b**) along the PIG calving front, looking toward the ice shelf. Both panels show temperature in colour relative to the *in situ* freezing point, salinity by black contours and the surface-referenced 27.75 isopycnal and potential temperature maximum by thick and thin white lines. Open circles in **b** show ice draft above the ridge crest (black dots) beneath the PIG, from airborne radar and Autosub measurements[11].

for the large PIG changes since the early 1990s, insight into the sub-ice shelf circulation can be gained from repeated measurements along the fast-moving region of the ice front (Fig. 2b). For example, 1994 CTD 92 was near 2009 CTD 16 (Fig. 1), where strong upwelling was roiling the sea surface, with brash ice being rapidly advected away from the highly fractured southern shear margin of the PIG. The T_θ/S relationship for CTD 16 is nearly linear over its entire length (Fig. 3b), with a slope of 2.63 indicating primarily a mixture of CDW and meltwater[15]. Temperatures 1–3 °C above freezing in that outflow showed that only about half the sensible heat available in CDW was being used to warm and melt the shelf ice. In addition to buoyant plumes, ice melting into sea water generates layered flows within the ambient density field[16], evident at this site as steps in the temperature and salinity profiles (Fig. 3b).

Meltwater content in the water column and its transport into and out of the sub-PIG cavity can be determined by techniques used near George VI Ice Shelf[17]. We first calculate profiles of meltwater from its temperature, salinity and dissolved oxygen tracers measured continuously on the CTD casts (see Methods). In 2009 the presence of meltwater was detected above ~700 dbar at all sites, at concentrations up to ~20 ppt, and the depth of the maximum concentration rose from ~400 dbar in the north to the sea surface at CTD 16 (Fig. 4a). Velocity estimates from geostrophic shear between CTD stations, referenced to an assumed level of no motion near the base of the meltwater layer, are adjusted to close the tracer budgets (see Methods). Near-surface data where surface contamination renders meltwater fractions uncertain (Fig. 4a) are excluded from these calculations. Inflows predominate in the north and at depth along much of the ice front, with outflows to the south mainly above 600 dbar (Fig. 4c). Total transport into the cavity is 400 mSv (0.4×10^6 m^3 s^{-1}), whereas outflow is larger by 2.26 mSv, equivalent to melting ~80 km^3 yr^{-1} of ice within the cavity. Alternate methods of deriving velocity estimates and balancing tracer budgets include referencing initial geostrophic currents to Lowered Acoustic Doppler Current Profiler (LADCP) measurements and using adjusted LADCP data alone (Supplementary Fig. S1f). The geostrophic calculations yield more consistent results (Supplementary Tables S1 and S2) with inherent spatial averaging of the velocity field, lower sensitivity to short-term variability and results more comparable to 1994 observations that lack LADCP data. Combining the several geostrophic seawater transport estimates gives a 396 ± 38 mSv inflow and a 2.40 ± 0.18 mSv larger outflow, equivalent to melting ~85 ± 6 km^3 yr^{-1} of ice.

Applying similar techniques to the more sparsely sampled 1994 ice front section yields a cavity inflow of 219 mSv, an outflow larger by 1.49 mSv, and melting of ~53 km^3 yr^{-1} (Fig. 4d and Supplementary Table S3). Combining that result with those from

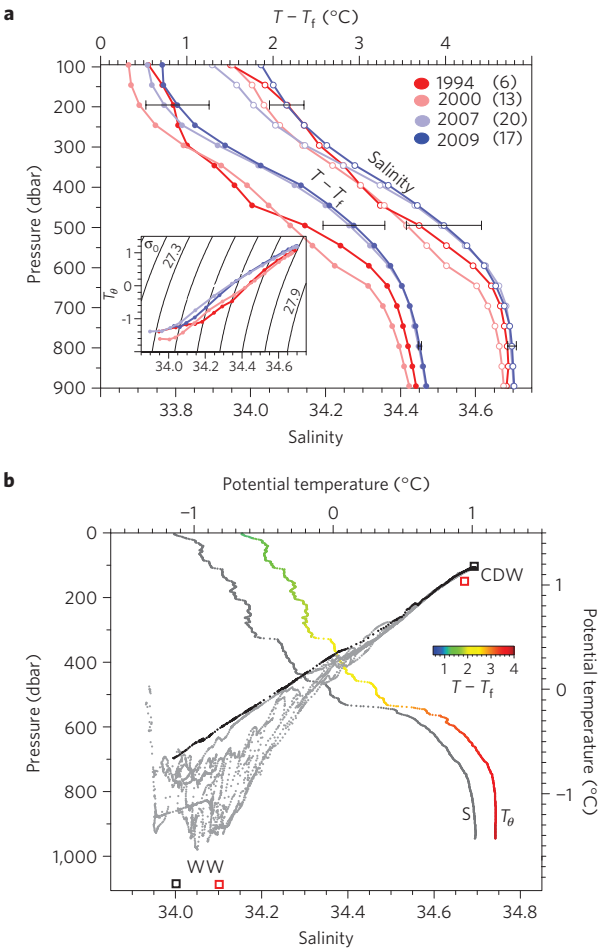

Figure 3 | Temperature and salinity in PIB. a, Cruise average, 50-dbar (~50 m) mean temperature above freezing ($T - T_f$) and salinity profiles from January–March 1994, 2000, 2007 and 2009 CTDs within 25 km (mean <10 km) of prior measurements (Fig. 1), with 1 σ (standard deviation) at 200, 500 and 800 dbar in 2009. Inset: the same data in T_θ (potential temperature)/Salinity space. **b**, T_θ (top scale, coloured in $T - T_f$) and salinity profiles at CTD 16, and T_θ (right scale)/salinity at CTDs 16 (black) and 17–23 (light grey) from Fig. 2b. Red and black boxes are 1994 and 2009 CDW and Winter Water properties (see Methods).

alternative assumptions gives an average 232 ± 35 mSv inflow, 1.59 ± 0.19 mSv larger outflow and equivalent melting of ~56 ± 7 km^3 yr^{-1}. A comparison using only 2009 CTDs closest to the 1994

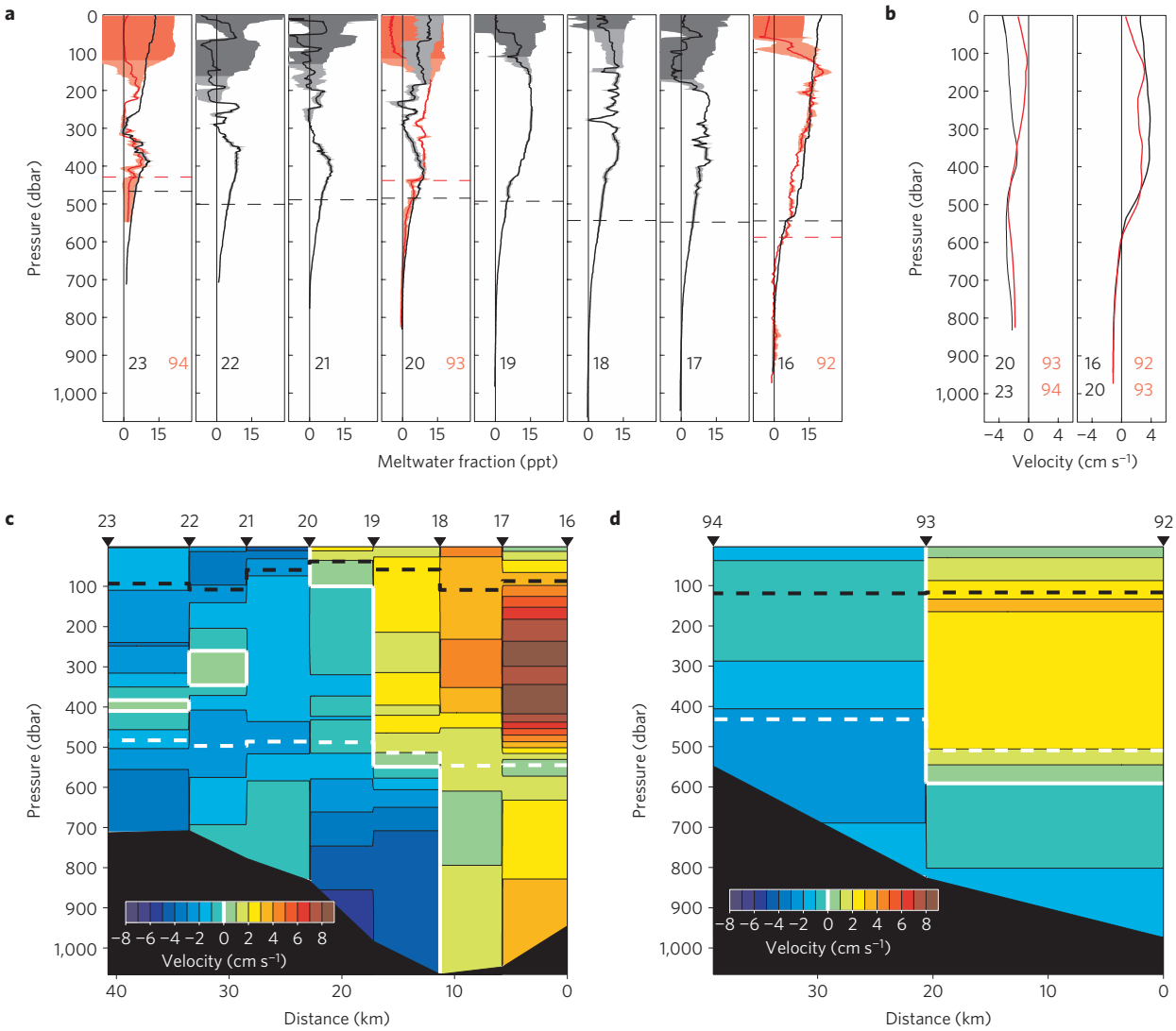

Figure 4 | Meltwater fractions and geostrophic current velocities near the PIG ice front. a, Meltwater profiles from ocean tracers[22] in 2009 (black) and 1994 (red), with means (solid lines) and range (1 σ, shaded, darker where σ is enlarged by surface effects at CTDs near the ice front (Fig. 1)). **b**, Adjusted geostrophic velocity profiles perpendicular to the ice front between gates defined by the indicated 1994 (red) and 2009 (black) profiles. **c**,**d**, Adjusted geostrophic velocities in 2009 and 1994 perpendicular to the ice front (positive denotes outflow). Dashed black and white lines show the excluded surface layer (shaded darker in **a**) and initial reference levels before adjustment (dashed lines in **a**).

profiles (Fig. 4b and Supplementary Table S1) indicates inflow of 376 mSv, outflow 2.20 mSv larger, and ~78 km^3 yr^{-1} of ice melt, showing that the stronger circulation and meltwater production in 2009 are not artefacts of profile spacing. The 1994 melt rates are higher than inferred from earlier assumptions[1], but significantly lower than in 2009, when similar meltwater fractions were being exported more rapidly from the cavity. The ~50% increase in melting roughly closes the glaciological budget, ice inflow across the grounding line having risen by a similar amount between 1996 and 2010 (ref. 18) while the ice shelf thinned by 70–80 m (ref. 10). A stronger sub-ice circulation is consistent with cavity growth and faster melting, the larger gap above the seafloor ridge enhancing cross-ridge ocean heat and meltwater transports, leveraging the small CDW temperature change.

The above measurements and calculations from the ice front sections would imply basal average melt rates of 33 m yr^{-1} in 2009 and 22 m yr^{-1} in 1994 if all net meltwater transport out of the cavity were derived from the fast-flowing ice in the ~70 × 35 km central region. However, some fraction of the meltwater will have come from the other, more slowly moving half of the ice shelf. In addition, the distribution of melting has a greater impact than its areal average on cavity shape, as can be inferred from the longitudinal ice shelf profile in Fig. 2a. Ice shelf velocity (~4 km yr^{-1}) changes little seaward of the grounding line[18], but the ice thins by ~500 m within 20 km of going afloat and only ~100 m in the next 50 km. These changes point to grounding zone melt rates an order of magnitude higher than beneath the shallower outer shelf ice, consistent with delivery of the warmest sea water to the deepest parts of the inner cavity. The meltwater adds buoyancy and cools the boundary layer along the ice shelf base, limiting direct contact between the ice and warmer CDW below.

Along with CDW variability in PIB, the sub-ice shelf ridge will have influenced ocean temperatures in the PIG grounding zone over recent decades. Meltwater production increased more slowly from 1994 to 2009 than seawater transport, with the fraction of sensible heat used for melting declining slightly. Faster circulation alone may not modify the utilization of oceanic sensible heat[19,20], but changes in cavity morphology such as the size and shape of the opening above the ridge and any deep sills it may contain will impact water column and boundary layer mixing processes.

Ice front temperatures in the 600–700 m interval that includes the ridge-clearing 27.75 isopycnal (CTDs 19–21 in Fig. 2b) average 3.5 °C above the *in situ* freezing point, close to the deepest Autosub measurement in the inner cavity (Fig. 2a), 100 m above the sea floor and ~5 km from a 950-m deep grounding line[11]. Ice front temperatures $T - T_f$ at that depth averaged 3.8 °C, largely a pressure effect that would also increase the measured inner cavity temperature to at least 3.6 °C nearer the grounding line. Although a deeper passage through or around the ridge, neither supported nor precluded by our data, might have initiated stronger basal melting, it makes little difference at present in grounding zone seawater thermal forcing. At 600–700 m in PIB, temperatures were ~0.2 °C higher in 2009 than in 1994 (Fig. 3a), a 6% increase in $T - T_f$ and 11% in $(T - T_f)^2$, theoretically the key parameter scaling melt rates beneath the larger ice shelves[21]. The much larger increase in circulation strength (~77%) and meltwater production (~50%) demonstrates the importance of factors besides far-field ocean temperature in controlling ice shelf mass balance.

In summary, repeated observations in PIB since 1994 display interannual variability and a small rise in CDW temperature and salinity, increasing upward to about the mean draft of the outer half of the PIG. Measurements along the PIG ice front reveal a substantial increase in meltwater production since 1994, driven more by a stronger cavity circulation than by the small increase in local CDW temperature. The faster seawater flow and growing gap above the ridge will have altered turbulence and mixing under the ice, but it remains to be determined how external changes, for example in winds or sea ice, may influence heat transport to the ice shelf grounding zone. A large inner cavity has developed in spite of accelerating ice flow, but grounding zone temperatures are now close to those in the outer cavity. If the cavity circulation steadies or weakens in response to changes in external or internal forcing, that could allow ice flux to close the inner cavity, regrounding the PIG in shallower water and slowing its speed. If ice velocity plateaus[18] while ocean circulation and meltwater production increase, then CDW could melt deeper into the West Antarctic Ice Sheet. Lengthy time series measurements and high-resolution modelling of these coupled air–sea-ice-trough systems are needed to better understand thermodynamic processes beneath the PIG and other thinning ice shelves.

Methods

Meltwater fraction calculations. At the calving front of PIG the summer water column consists mainly of CDW overlain by surface water, mixtures of the two, and meltwater from the ice shelf[1,3,22]. The surface water includes remnant 'Winter Water' (WW) layers beneath and interspersed with waters modified by summer sea surface processes, and in some locations (CTD 16, for example) by upwelled outflows from beneath the ice shelf. Meltwater added to mixtures of CDW and WW can be identified using three composite tracers derived from CTD-measured parameters:

$$\psi^{2,1} = (\chi^2 - \chi^2_{\mathrm{CDW}}) - (\chi^1 - \chi^1_{\mathrm{CDW}})\left(\frac{\chi^2_{\mathrm{WW}} - \chi^2_{\mathrm{CDW}}}{\chi^1_{\mathrm{WW}} - \chi^1_{\mathrm{CDW}}}\right)$$

where χ^i represents potential temperature, salinity or dissolved oxygen and subscripts indicate defined water mass characteristics[22]. Temporal changes in the water mass properties (Fig. 3a, for example) require that the core characteristics be separately defined for each year (Fig. 3b). Any non-zero value of the composite tracer can be directly related to meltwater fraction:

$$\varphi = \frac{\psi^{2,1}_{\mathrm{mix}}}{\psi^{2,1}_{\mathrm{melt}}}$$

where the denominator is the composite tracer value in pure meltwater[22]. Near-surface processes contaminate the composite tracers in different ways, but those discrepancies can be used to indicate where the derived ice shelf meltwater fraction is suspect.

Transport calculations. Assuming that all transport into and out of the cavity must cross our ice front section, the difference between inflow and outflow will equal the addition of meltwater, M_{melt}, from the ice shelf base[17]. We estimate the total transport across the section as the sum of n individual transports, $(M_{\mathrm{out}} - M_{\mathrm{in}})$, between the $n+1$ adjacent CTD stations:

$$\sum_{j=1}^{n} (M_{\mathrm{out}} - M_{\mathrm{in}})_j = M_{\mathrm{melt}}$$

Assuming that cavity properties are in steady state, a similar equation can be written for the transport of each tracer across the section:

$$\sum_{j=1}^{n} \left[(M\chi)_{\mathrm{out}} - (M\chi)_{\mathrm{in}}\right]_j = M_{\mathrm{melt}}\chi_{\mathrm{melt}}$$

and because the tracer value in the meltwater is constant, the unknown melt transport can be eliminated[17]

$$\sum_{j=1}^{n} \{[M(\chi - \chi_{\mathrm{melt}})]_{\mathrm{out}} - [M(\chi - \chi_{\mathrm{melt}})]_{\mathrm{in}}\}_j = 0 \quad (1)$$

The steady state assumption is justified because property variability below the surface layer, excluded from the budget, is small on the monthly timescale over which cavity waters are renewed. Transports between adjacent CTD stations are calculated by depth-integrating the product of tracer concentration and velocity normal to the line joining the stations:

$$\left\{[M(\chi - \chi_{\mathrm{melt}})]_{\mathrm{out}} - [M(\chi - \chi_{\mathrm{melt}})]_{\mathrm{in}}\right\}_j = \frac{1}{g}\left\{\int_{P_{\mathrm{bot}}}^{P_{\mathrm{top}}} \bar{v}(p)\left[\bar{\chi}(p) - \chi_{\mathrm{melt}}\right]\Delta x(p)\, dp\right\}_j$$

where overbars indicate averages over the width, Δx, between stations, g is gravity, v is velocity and p is pressure[17]. The width-averaged velocity is derived from an estimate of the geostrophic shear between stations:

$$f\frac{\partial \bar{v}}{\partial p} = -\left.\frac{\partial \alpha}{\partial x}\right|_p \quad (2)$$

where α is the specific volume, calculated from measurements of temperature, salinity and pressure. Derivation of the absolute velocity from (2) introduces one unknown constant of integration for each station pair. To define these constants we initially assume that pure CDW/WW mixtures are more likely to be flowing into the cavity, while water with an admixture of melt is more likely to be flowing away from the ice, and accordingly set the velocity to zero near the base of the melt-enriched layer (Fig. 4a).

In general the transports thus derived will not satisfy the summation in equation (1), because the sampling is imperfect, meltwater from other sources could be entering the cavity, and the assumed geostrophic balance may not hold. But the budgets can be closed by adding a constant velocity adjustment to each profile[17]:

$$\sum_{j=1}^{n} \frac{v_j^{adj}}{g}\left\{\int_{P_{\mathrm{bot}}}^{P_{\mathrm{top}}} \left[\bar{\chi}(p) - \chi_{\mathrm{melt}}\right]\Delta x(p)\, dp\right\}_j$$

$$+\sum_{j=1}^{n} \frac{1}{g}\left\{\int_{P_{\mathrm{bot}}}^{P_{\mathrm{top}}} \bar{v}(p)\left[\bar{\chi}(p) - \chi_{\mathrm{melt}}\right]\Delta x(p)\, dp\right\}_j = 0$$

Equations for temperature, salinity and dissolved oxygen each contain seven unknown velocity adjustments for the 2009 section. This under-determined problem has many possible solutions, and we choose the one closest to our initial assumption that minimizes the sum of the squares of the velocity adjustments[17,23]. For the 1994 section, with only two velocity profiles, the problem is over-determined and the chosen solution minimizes the sum of the squares of the net tracer transports. This strategy retains the vertical velocity structure derived from equation (2) while allowing arbitrary shifts in the depth-mean currents for each station pair. In both cases the solution changes the initial assumption of a pure overturning circulation into one showing a small but coherent depth-mean circulation with inflow in the north and net outflow in the south.

Received 1 December 2010; accepted 20 May 2011; published online 26 June 2011; corrected online 29 June 2011

References

1. Jacobs, S. S., Hellmer, H. H. & Jenkins, A. Antarctic ice sheet melting in the southeast Pacific. *Geophys. Res. Lett.* **23,** 957–960 (1996).
2. Jenkins, A. *et al.* Glaciological and oceanographic evidence of high melt rates beneath Pine Island Glacier, West Antarctica. *J. Glaciol.* **43,** 114–121 (1997).
3. Hellmer, H. H., Jacobs, S. S. & Jenkins, A. in *Ocean Erosion of a Fast-Moving Antarctic Glacier in the Amundsen Sea* 83–99 (Ant. Res. Ser., 75, AGU, 1998).
4. Rignot, E. Fast recession of a West Antarctic glacier. *Science* **281,** 549–551 (1998).

5. Shepherd, A., Wingham, D. J., Mansley, J. A. D. & Corr, H. F. J. Inland thinning of Pine Island Glacier, West Antarctica. *Science* **291,** 862–864 (2001).
6. Joughin, I., Rignot, E., Rosanova, C. E., Lucchitta, B. K. & Bohlander, J. Timing of recent accelerations of Pine Island Glacier, Antarctica. *Geophys. Res. Lett.* **30,** 1706 (2003).
7. Shepherd, A., Wingham, D. J. & Rignot, E. Warm ocean is eroding West Antarctic Ice Sheet. *Geophys. Res. Lett.* **31,** L23402 (2004).
8. Payne, A. *et al.* Numerical modeling of ocean–ice interactions under Pine Island Bay's ice shelf. *J. Geophys. Res.* **112,** C10019 (2007).
9. Rignot, E. Changes in West Antarctic ice stream dynamics observed with ALOS PALSAR data. *Geophys. Res. Lett.* **35,** L12505 (2008).
10. Wingham, D. J., Wallis, D. W. & Shepherd, A. Spatial and temporal evolution of Pine Island Glacier thinning, 1995–2006. *Geophys. Res. Lett.* **36,** L17501 (2009).
11. Jenkins, A. *et al.* Observations beneath Pine Island Glacier in West Antarctica and implications for its retreat. *Nature Geosci.* **3,** 468–472 (2010).
12. Dinniman, M. S., Klinck, J. M. & Smith, W. O. Jr Cross-shelf exchange in a model of the Ross Sea circulation and biogeochemistry. *Deep-Sea Res. II* **50,** 3103–3120 (2003).
13. Walker, D. P. *et al.* Oceanic heat transport onto the Amundsen Sea shelf through a submarine glacial trough. *Geophys. Res. Lett.* **34,** L02602 (2007).
14. Thoma, M., Jenkins, A., Holland, D. M. & Jacobs, S. S. Modelling Circumpolar Deep Water intrusions on the Amundsen Sea continental shelf, Antarctica. *Geophys. Res. Lett.* **35,** L18602 (2008).
15. Gade, H. G. Melting of ice in seawater: A primitive model with application to the Antarctic ice shelf and icebergs. *J. Phys. Oceanogr.* **9,** 189–198 (1979).
16. Jacobs, S. S., Huppert, H. E., Holdsworth, G. & Drewry, D. J. Thermohaline steps induced by melting of the Erebus Glacier Tongue. *J. Geophys. Res.* **86,** 6547–6555 (1981).
17. Jenkins, A. & Jacobs, S. S. Circulation and melting beneath George VI Ice Shelf, Antarctica. *J. Geophys. Res.* **113,** C04013 (2008).
18. Joughin, I., Smith, B. E. & Holland, D. M. Sensitivity of 21st century sea level to ocean-induced thinning of Pine Island Glacier, Antarctica. *Geophys. Res. Lett.* **37,** L20502 (2010).
19. Holland, P. R., Jenkins, A. & Holland, D. M. The response of ice-shelf basal melting to variation in ocean temperature. *J. Clim.* **21,** 2558–2572 (2008).
20. Little, C. M., Gnanadesikan, A. & Oppenheimer, M. How ice shelf morphology controls basal melting. *J. Geophys. Res.* **114,** C12007 (2009).
21. MacAyeal, D. R. Thermohaline circulation below the Ross Ice Shelf: A consequence of tidally induced vertical mixing and basal melting. *J. Geophys. Res.* **89,** 597–606 (1984).
22. Jenkins, A. The impact of melting ice on ocean waters. *J. Phys. Oceanogr.* **29,** 2370–2381 (1999).
23. Wunsch, C. The North Atlantic general circulation west of 50° W determined by inverse methods. *Rev. Geophys. Space Phys.* **16,** 583–620 (1978).
24. Nitsche, F. O., Jacobs, S. S., Larter, R. D. & Gohl, K. Bathymetry of the Amundsen Sea continental shelf: Implications for geology, oceanography and glaciology. *Geochem. Geophys. Geosyst.* **8,** Q100009 (2007).

Acknowledgements

We have been ably assisted by many colleagues aboard ship and at several institutions in the acquisition, analysis and presentation of data used in this study. The NSF, NOAA and NERC have supported this work, currently under grants ANT06-32282, NA080AR4320912, and NE/G001367/1.

Author contributions

S.S.J. and A.J. proposed the research, analysed the results and wrote the text. C.F.G. and P.D. processed the data. C.F.G., P.D. and A.J. prepared the figures. All authors read and commented on the paper.

Additional information

The authors declare no competing financial interests. Supplementary information accompanies this paper on www.nature.com/naturegeoscience. Reprints and permissions information is available online at http://www.nature.com/reprints. Correspondence and requests for materials should be addressed to S.S.J. or A.J.

ERRATUM

Stronger ocean circulation and increased melting under Pine Island Glacier ice shelf

Stanley S. Jacobs, Adrian Jenkins, Claudia F. Giulivi and Pierre Dutrieux

Nature Geoscience doi:10.1038/ngeo1188 (2011); published online 26 June 2011; corrected online: 29 June 2011.

In the version of this Letter originally published online, Fig. 4b–d were incorrectly described in the caption. This error has now been corrected in all versions of the Letter.